國 立 交 通 大 學
奈 米 科 技 研 究 所

碩 士 論 文

鐵-18 at.%鋁-10 at.%鈦合金之相變化

Phase Transformations in an Fe-18 at.%Al-10 at.%Ti Alloy

研究生　：劉哲郎
指導教授：劉增豐 教授
朝春光 教授

中 華 民 國 九 十 六 年 七 月

Fe-18 at.%Al-10 at.%Ti 之合金相變化

Phase Transformations in an

Fe-18 at.%Al-10 at.%Ti Alloy.

研 究 生：劉哲郎　　Student：Che-Lang Liu

指導教授：劉增豐 博士　　Advisor：Dr. T. F. Liu

朝春光 博士　　Advisor：Dr. C. G. Chao

國 立 交 通 大 學

奈 米 科 技 研 究 所

碩 士 論 文

A Thesis

Submitted to Department of Nano-Technology

College of Engineering

National Chiao Tung University

In partial Fulfillment of the Requirements

For the Degree of

Master

in

Materials Science and Engineering

July 2007

Hsinchu, Taiwan, Republic of China

中華民國九十六年七月

致謝

感謝指導教授**劉增豐**博士兩年來細心的照顧和敦敦教誨，尤其碩士論文上的傾心幫忙，才能使得學生能順利完成論文，在此對吾師**劉增豐**教授以及師母**林美惠**老師致上最大的敬意與謝意。

此外，感謝實驗室的學長學弟們，因為有了你們，實驗室總是充滿了溫暖與歡樂。尤其感謝**蘇俊偉**學長，不論是在 TEM 的操作上或是充滿拼勁的實驗精神，都讓我獲益良多，也因為學長的幫忙，碩士生涯才會如此順利。感謝各位學長：**王承舜**、**蔡國棟**、**段逸軒**、**林志龍**、**黃世陽**、**陳信良**學長們在課業上的指導還有生活上照顧；同學**陳柏至**、**蔡雨霖**、**王浩仰**、**黃敬恆**的相互扶持；還有學弟**林欣龍**在實驗上的協助。我將會懷念和你們一起做實驗的生活。在本實驗室上下一心的情況下得以完成本篇論文。

最後，僅將碩士論文的成果，獻給我最親愛的父母親，以及哥哥，由於你們的包容與支持，讓我能夠順利的取得碩士學位。

中　文　摘　要

我們利用光學顯微鏡(OM)、穿透式電子顯微鏡(TEM)和 X 光能量散佈分析儀(EDS)，研究 Fe-18at.%Al-10at.%Ti 合金的相變化。

Fe-18at.%Al-10at.%Ti 合金在淬火狀態下的顯微結構為(A2+$D0_3$)相的混合。其中 $D0_3$ 相是經由 A2 → B2 → (A2+$D0_3$)之連續規律化的過程而產生。當我們將此合金在 700℃至 1100℃的溫度範圍內施以不同時間的時效處理後發現，此合金隨著溫度的增加其一系列相變化過程為 A2+$D0_3$→A2+$D0_3$+C14→B2+C14→A2+C14→A2；值得一提的是，這一實驗結果從未被其他學者觀察過。此外，當此合金在 800℃作 1 小時的時效處理後，經過擇區繞射圖我們觀察到基底的(A2+$D0_3$)相和 C14 相會有以下的方向關係 $(0\,0\,0\,1)_{C14}//(\bar{1}\,\bar{1}\,2)_m$, $(\bar{1}\,1\,0\,0)_{C14}//(\bar{1}\,1\,0)_m$, $(1\,1\,\bar{2}\,0)_{C14}//(1\,1\,1)_m$，這一實驗結果在 Fe-Al-Ti 合金中也從未被發現過。

Abstract

Phase transformations in an Fe-20at.%Al-8at.%Ti alloy have been examined by means of optical microscopy (OM), transmission electron microscopy (TEM) and energy-dispersive X-ray spectrometer (EDS).

In the as-quenched condition, the microstructure of the Fe - 18at.%Al - 10at.%Ti alloy was a mixture of (A2+$D0_3$) phases and the $D0_3$ phase was formed by an A2 → B2 → (A2+$D0_3$) continuous ordering transition during quenching. When the as-quenched alloy was aged at temperatures ranging from 700℃ to 1100℃, the phase transition sequence as the aging temperature increased was found to be A2+$D0_3$→A2+$D0_3$+C14→B2+C14→A2+C14→A2. It is noted here that this phase transition has never been observed by other workers in the Fe-Al-Ti alloys before. In addition, when the present alloy was aged at 850℃, the orientation relationship between the C14 precipitate and (A2+$D0_3$) matrix was determined to be $(0\,0\,0\,1)_{C14}//(\bar{1}\,\bar{1}\,2)_m$, $(\bar{1}\,1\,0\,0)_{C14}//(\bar{1}\,1\,0)_m$, $(1\,1\,\bar{2}\,0)_{C14}//(1\,1\,1)_m$ analysed by the above diffraction patterns. This orientation relationship between the C14 precipitate and A2, $D0_3$ or B2 matrix has never been reported by other workers in the Fe-Al-Ti alloy systems before.

Contents

List of Figures

List of Table

Introduction

The microstructures of the Fe-Al binary alloys have been studied by many workers [1-3]. In their studies, it is seen that only three phase, namely disordered A2 (ferrite), ordered B2 (FeAl) and $D0_3$, could be found in the Fe-rich portion of Fe-Al binary alloys as shown in Figure 1. Fe-Al alloys based on Fe_3Al exhibit an irregular peak in yield stress at an intermediate temperature, which is attractive for high-temperature application. The reason is well-known relation with the $D0_3 \rightarrow$ B2 ordering transition temperature. Efforts to improve the strength of Fe-Al alloy systems at elevated temperatures have been looked for by many workers from the point of the critical temperature T_c for the $D0_3 \rightarrow$ B2 transition [4,5]. It is found that addition of a third element to Fe-Al binary alloys would increase the point of the critical temperature T_c. The addition of ternary alloying elements with the intention of increasing the $D0_3 \rightarrow$ B2 transition temperature $T_c^{D03 \rightarrow B2}$ has been studied in detail. In 1995, Anthony and Fultz found that the transition temperature increased approximately linear with increasing solute concentration for a number of different transition metals (Ti, V, Cr, Zr, Mo, Hf, Ta and W). Based on their studies, the addition of Ti results in a significantly amount increasing $T_c^{D03 \rightarrow B2}$

about 60°C /at.%. Furthermore, effects of Ti addition on the microstructures of the Fe-rich Fe-Al binary alloys have been extensively studied by many workers [6-8]. According to these studies, it can be generally concluded that the addition of Ti in the Fe-Al binary alloys would not only pronouncedly raise the A2+$D0_3$ (or $D0_3$)→B2→A2 transition temperatures but also significantly expand the (A2+$D0_3$) phase field. The limited stability of the $D0_3$ structure can be increased from about 550°C for binary Fe-Al alloys with 25 at.% Al to approximate 825°C for adding 5 at.% Ti on the Fe_3Al alloy. As a result, a significant increase in the strength and hardness of Fe-Al-Ti alloys at elevated temperatures was eventually achieved by raising the critical temperature $T_c^{D03 \rightarrow B2}$ transition.

Previous studies have found that if Ti content was increased higher than 7 at.% or above, the C14 precipitates could be detected at grain boundaries and within matrix in the aged Fe-Al-Ti alloys [9,10]. The C14 precipitate has a hexagonal structure with lattice parameters a=0.5038 nm and c=0.8193 nm. Some workers pointed out that the strengthening mechanism apart from the solid solution strengthening is to increase the stability of the Fe_2(Fe,Ti)Al ($D0_3$ or $L2_1$) phase to higher temperatures. There is another possibility proposed by the precipitation of the C14 precipitate.

Based on the previous studies, it is clearly seen that although the phase transformations in the Fe-Al-Ti alloys have been widely studied, most of the observations were only focused on the Fe-Al-Ti alloys with lower Ti content. Information about the microstructural development of the Fe-Al-Ti alloys with Ti > 5 at.% is very deficient. Therefore, the purpose of the present study is to investigate the phase transformations of the Fe-18 at.%Al- 10 at.%Ti alloy.

Experimental procedure

(A) Alloy Preparation

The alloy, Fe-18 at.% Al-10 at.% Ti, was prepared in a vacuum induction furnace by using 99.9% iron, 99.9% aluminum and 99.9% titanium. The melt was chill cast into a 30 × 50 × 200-mm-copper mold. After being homogenized at 1250°C for 48 hours, the ingot was sectioned into 2-mm-thick slices. These slices were subsequently solution heat-treated at 1150°C for 1 hour and then rapidly quenched into room-temperature water. The aging processes were performed at temperatures ranging from 700°C to 1100°C in a vacuum heat-treated furnace for various times and then quenched into room-temperature water rapidly.

(B)Optical Microscopy (OM)

The optical microscopy specimens were prepared as the following steps: sections, mounting, rough polishing, fine polishing and finally etching with 60% CH_3COOH, 30% HNO_3 and 10% HCl.

(C) Transmission Electron Microscopy (TEM)

The electron microscopy specimens were prepared by a double-jet electropolisher with an electrolyte of 67% methanol and 33% nitric acid. The polishing temperature was kept in the range from -30°C to -20°C, and the current density was kept in the range from 4.0×10^4 to 6.0×10^4 A/m^2. Electron microscopy was performed on a JEOL JEM-2000FX scanning transmission electron microscope operating at 200kV. This microscope was equipped with a Link ISIS 300 energy-dispersive X-ray spectrometer (EDS) for chemical analysis. Quantitative analyses of elemental concentrations for Fe, Al and Ti were made with the aid of a Cliff-Lorimer Ratio Thin Section method.

Results

Figure 1 is an optical micrograph of the alloy after being solution heated at 1150℃ for 1 hour and then quenched into water. Figure 2(a) is a bright-field(BF) electron micrograph of the as-quenched alloy. Figures 2(b) and 2(c) are two selected-area diffraction pattern(SADP) taken from the matrix in Figure 2(a), exhibiting the superlattice reflection spots of the ordered $D0_3$ phase [11]. The zone axe are [100] and [110], respectively. Figure 2(d) is a $(\bar{1}11)$ $D0_3$ dark-field (DF) electron micrograph of the as-quenched alloy, revealing the presence of extremely fine $D0_3$ domains. Figure 2(e), a (002) $D0_3$ DF electron micrograph, shows the presence of small B2 domains with a/4<111> APBs. Since the sizes of both $D0_3$ and B2 domains are very small, it is deduced that the B2 and $D0_3$ domains were formed during quenching by an ordering transition [12]. In Figure 2(e), it is also seen that a high density of disordered A2 phase (dark contrast) is present within the B2 domains. It can be concluded from the above observations that in the as-quenched condition, the microstructure of the alloy was a mixture of ($A2+D0_3$) phases, which were formed by an A2 → B2 → ($A2+D0_3$) ordering transition during quenching. This result is similar to that observed by other workers in the Fe-(18~22.5) at.% Al-5 at.% Ti alloys [5].

Figures 3(a) and 3(b) are $(\bar{1}11)$ and (002) DF electron micrographs of the

alloy aged at 700℃ for 6 hours and then quenched. It is seen that the $D0_3$ domains grew rapidly. Figure 3(b) is a DF electron micrograph obtained by use of the (002) superlattice reflection in [001] zone, revealing that the $D0_3$ domains were aligned along <100> directions. This feature is also similar to that observed by Mendiratta *et al.* in the aged Fe-Al-Ti alloy [5]. When the aging time was increased to 12 hours, the $D0_3$ domains continued to grow and the morphology changed from cubic to granular shape, as shown in Figures 4(a) and (b). Figures 4(a) and (b) are $(\bar{1}11)$ and (002) $D0_3$ DF electron micrographs, clearly showing that these two figures are morphologically identical. It is well-known that the (002) reflection spot comes from both the B2 and $D0_3$ phases, while the $(\bar{1}11)$ reflection spot comes only from $D0_3$ phase. Therefore, the bright particles presented in Figures 4(a) and (b) are considered to be $D0_3$ phase. Accordingly, the microstructure of the alloy was a mixture of ($A2+D0_3$) phases.

Figure 5(a) is a bright-field (BF) electron micrograph of the alloy aged at 800˚C for 0.5 hour. It is clear that there are some rod-like precipitates within the matrix. Figures 5(b) through (d) are three different SADPs taken from an area including the precipitate marked as “C” in Figure 5(a). By analyzing these values of interplanar spacings and angles between reciprocal vectors of the

diffraction spots in these SADPs, the crystal structure of the rod-like precipitate was determined to be have a hexagonal cubic primitive structure with lattice parameters a=0.499 nm and c=0.793 nm. The crystallographic normals shown in Figures 5(b) through (d) are [0001], $[01\bar{1}0]$ and $[2\bar{1}\bar{1}0]$, respectively. It is clear that the rod-like precipitate is surrounded by free-zone. Fig 5(e) is the rod-like precipitate DF. Figures 5(f) and (g) are $(\bar{1}11)$ and (002) $D0_3$ DF electron micrographs, revealing that extremely fine $D0_3$ precipitates were formed within the matrix. The extremely fine $D0_3$ precipitates which were formed by an A2 → B2 → (A2+$D0_3$) ordering transition during quenching. When the aging time was increased, cuboidal $D0_3$ particles started to occur contiguous to the C14 precipitate. Figure 6(a) is a bright-field (BF) electron micrograph of the alloy aged at 800°C for 1 h. Figures 6(b) through (d) demonstrate three different SADPs taken from an area including the rod-like precipitate in Figure 6(a) and its surrounding matrix. The crystallographic normals of the (A2+$D0_3$) matrix are $[1\,1\,1]_m$, $[1\,1\,0]_m$ and $[\bar{1}\,\bar{1}\,2]_m$, respectively. In addition to the spots corresponding to the (A2+$D0_3$) phase, the diffraction patterns also consist of small spots caused by the presence of precipitate. Analyses by the above diffraction patterns, the orientation relationship between the C14 precipitate and (A2+$D0_3$) matrix was $(0\,0\,0\,1)_{C14}//(\bar{1}\,\bar{1}\,2)_m$, $(\bar{1}\,1\,0\,0)_{C14}//(\bar{1}\,1\,0)_m$,

$(1\,1\,\bar{2}\,0)_{C14}//(1\,1\,1)_m$. It is worthy to note that the orientation relationship between the C14 precipitate and A2, $D0_3$ or B2 matrix has never been reported by other workers in the Fe-Al-Ti alloy systems before. Figures 6(e) is $(\bar{1}11)$ $D0_3$ DF electron micrographs, clearly revealing that three types of $D0_3$ particles could be detected: one is the granular-like $D0_3$ particles within the matrix; another is the cuboidal $D0_3$ particles contiguous to the C14 precipitate. Because the size of these two types of $D0_3$ particles is larger than that observed in the as-quenched alloy. It is therefore reasonable to believe that these two types of the $D0_3$ particles were existent at the aging temperature. The other is the extremely fine $D0_3$ particles, which was formed within the A2 matrix by an A2 → B2 → (A2+$D0_3$) ordering transition during quenching. It is concluded from the above observations that the microstructure of the alloy present at 800˚C was a mixture of (A2+$D0_3$+C14) phases.

Figure 7(a) and (b) are bright-field and C14 DF electron micrographs of the alloy aged at 900˚C for 6 hours, revealing the presence of the rod-like C14 precipitate. Transmission electron microscopy examinations indicated that extremely fine $D0_3$ domains observed within the matrix, as shown in Figure 7(c). This indicates that the extremely fine $D0_3$ domains were formed through an ordering transition during quenching from the aging temperature; otherwise, the

$D0_3$ domains should grow at the aging temperature. Figure 7(d), (002) $D0_3$ DF electron micrograph of the same area as Figure 7(c), shows that along with the growth of the B2 domains, the a/4<111> APBs have gradually disappeared. Furthermore, it could be also seen that the dark contrast within the B2 domains was observed because of the presence of disordered A2 phase; if not so, there would be not any dark contrast in a (002) DF electron micrograph. It indicates that the microstructure of the alloy present at 900°C should be B2 phase and the extremely fine $D0_3$ domains were formed by a B2 → (A2+$D0_3$) ordering transition during quenching. From the above observations, the microstructure of the present alloy at 900°C was a mixture of (B2+C14) phases.

Figure 8(a) is a bright-field electron micrograph of the alloy aged at 1000°C for 1 hour. Transmission electron microscopy examinations indicated that besides the C14 precipitates, only quenched-in extremely fine $D0_3$ domains and small B2 domains were present within the matrix. An example is shown in Figure 8(c) and (d). It means that the stable microstructure of the present alloy at 1000°C was a mixture of (A2+C14) phases.

Progressively higher temperature aging and quenching experiments indicated the mixture of (A2+C14) phases could be maintained up to 1050°C. However, when the alloy was aged at 1100°C and then quenched, the C14

precipitates disappeared and only quenched-in extremely fine $D0_3$ domains and small B2 domains (the sizes being comparable to those observed in the as-quenched alloy) could be detected, as illustrated in Figure 9(a) through 9(c). This indicates that the microstructure of the present alloy existing at 1100°C or above should be the single disordered A2 phase.

Based on the above experimental results, it is concluded that with increasing the aging temperature from 700°C to 1100°C, the phase transition sequence in the present alloy is $A2+D0_3 \rightarrow A2+D0_3+C14 \rightarrow B2+C14 \rightarrow A2+C14 \rightarrow A2$.

Discussion

According to the above observations, some important features of the present study are worthy of note as follows:

(Ⅰ) When the present alloy was aged at 800°C for 1 hour, the cuboidal $D0_3$ particles were observed to appear contiguous to the C14 precipitate. It is a noticeable feature in the present study, which has never been observed by other workers in the Fe-Al-Ti alloy systems. In order to clarify this feature, an STEM-EDS analyses were undertaken. Figures 10(a) through (d) are four typical EDS spectra taken from a granular-like $D0_3$ particle within the matrix, a cuboidal $D0_3$ particle contiguous to the C14 precipitate, C14 precipitate and the (A2+$D0_3$) matrix in the alloy aged at 800°C for 1 hour, respectively. The average concentrations of alloying elements obtained by analyzing several EDS spectra of each phase are listed in Table 1. For comparasion, the chemical compositions of the as-quenched alloy are also listed in Table 1. It is seen in Figure 10(c) and Table 1 that the concentration of Ti in the C14 precipitate can be increased up to 25.65 at.%, which is obviously higher than that in the as-quenched alloy. On the contrary, the Al concentration is much lower than that in the as-quenched alloy. It implies that when the C14 precipitates grew in the matrix, the concentration of

Al of the matrix in the vicinity of the C14 precipitates would be increased. This result corresponds to the concentration of Al in Figure 10(b) and Table 1. According to the phase diagram of Fe-Al binary alloys, it is seen that the microstructure of an Fe-25.96 at.% Al alloy should be a single $D0_3$ phase below 550°C. Furthermore, it is believed from the STEM-EDS analysis that 6.54 at.% Ti is enough to permit the cuboidal $D0_3$ to form contiguous to the C14 precipitate at 800°C, as observed in Figure 6(e).

In the Fe-Al binary alloy, it is well-known that the $D0_3$ phase was formed by an ordering transition during quenching at Al > 22.1 at.%. Moreover, it was reported that the effect of Ti addition on the Fe-Al alloy systems not only increased the $D0_3 \rightarrow B2$ transition temperature but also expanded the $(A2+D0_3)$ phase regions of the Fe-Al alloy systems in the previous studies of the Fe-Al-Ti alloys. However, the $A2 \rightarrow A2+D0_3$ ordering transition could be detected and the Al concentration in the $(A2+D0_3)$ phases was examined to be 16.99 at.% only, as shown in Figure 10(d). Therefore, it is believed that the solubility of 4.76 at.% Ti within the A2 phase should be favorable to occur $B2 \rightarrow D0_3$ ordering transition during quenching from 800°C.

(Ⅱ) Although the C14 precipitate has been extensively reported to exist by many works in the aged Fe-Al-X (X=Nb, Zr or Ta) alloys system [13], there is

only one article concerning the orientation relationship between the C14 precipitate and matrix. In 2005, D.G. Morris *et al*. reported that there were several approximate orientation relationships between the C14 precipitate and the $D0_3$ matrix in the aged Fe-25Al-2Nb alloy [35], namely:

$\{\bar{1}\,0\,1\,0\}_{C14}//\{\bar{1}\,0\,1\}_m$, $<1\,\bar{2}\,1\,0>_{C14} \approx <0\,1\,0>_m$ and $<0\,0\,0\,1>_{C14} \approx <1\,0\,1>_m$.

However, the only exact relationship was $\{\bar{1}\,0\,1\,0\}_{C14}//\{\bar{1}\,0\,1\}_m$ and the others were approximate with a difference of a few degrees (3~5°).

Recently, the present workers performed TEM observations on the phase transformations of the Fe-Al-Ti alloy systems. Based on our experimental results, it is found that the orientation relationship between the C14 precipitate and (A2+$D0_3$) matrix was determined as follows: $(0\,0\,0\,1)_{C14}//(\bar{1}\,\bar{1}\,2)_m$, $(\bar{1}\,1\,0\,0)_{C14}//(\bar{1}\,1\,0)_m$, $(1\,1\,\bar{2}\,0)_{C14}//(1\,1\,1)_m$ [34]. It is worthwhile to note here that this orientation relationship has never been reported by previous workers in the Fe-Al-Ti alloy systems before. Compared with present work, it is worthy to note that only $(\bar{1}\,1\,0\,0)_{C14}//(\bar{1}\,1\,0)_m$ is indeed in agreement with Morris *et al.* but the other relationship are discrepant. One possible reason for the apparent difference between the two works is that the different elements formed the different lattice parameter of the C14 precipitate.

Conclusions

In the present study, the phase transformations in the Fe-18 at.% Al-10 at.% Ti alloy have been examined. The experimental results obtained are as follows：

(1). In the as-quenched condition, the microstructure of the Fe-18 at.%Al-10 at.%Ti alloy was a mixture of (A2+$D0_3$) phases, which were formed during quenching by an A2 → B2 → (A2+$D0_3$) ordering transition.

(2). When the alloy was aged at 700˚C, the $D0_3$ precipitates grew aligned along <100> directions rapidly. With increasing aging time, the $D0_3$ domains continued to grow and the morphology changed from cuboidal to granular shape.

(3). When the alloy was aged at 800˚C for 0.5 hour, the rod-like C14 precipitates could be observed within the (A2+$D0_3$) matrix. Along with the growth of the C14 precipitates, the surrounding region would be enriched in aluminum. The enrichment of aluminum would enhance the formation of the cuboidal $D0_3$ particles at the regions contiguous to the C14 precipitates.

(4). When the as-quenched alloy was aged at temperature ranging from 750˚C to 1100˚C, the phase transformation sequence as the aging temperature increased was found to be (A2+$D0_3$) → (A2+$D0_3$+C14) → (B2+C14) →

(A2+C14) → A2.

(5). The orientation relationship between the C14 precipitate and ($A2+D0_3$) matrix was determined to be $(0\,0\,0\,1)_{C14}//(\bar{1}\,\bar{1}\,2)_m$, $(\bar{1}\,1\,0\,0)_{C14}//(\bar{1}\,1\,0)_m$, $(1\,1\,\bar{2}\,0)_{C14}//(1\,1\,1)_m$, which has never been reported in the Fe-Al-Ti alloys system before.

References

1. M. Palm : Intermetallics,13, 1286(2005)
2. O. Ikeda, I.Ohnuma, R. Kainuma, K. Ishida: Acta, 9, 755(2001)
3. S. Zuqing, Y. Wangyue, S. Lizhen, H. Yuanding, Z. Baisheng, Y. Jilian : Mater. Sci. & Eng., A258, 69(1998)
4. Y. Nishino, S.Asano, T. Ogawa : Mater. Sci. & Eng., A234-236, 271(1997)
5. M.G. Mendiratta, S.K. Ehlers, H.A. Lipsitt : Metal Trans A, 18A, 509(1987)
6. F.Dobes, Petr Kratochvi, K. Milicka : Intermetallics, 14, 1199(2006)
7. B. Pandey, P.M.G. Nambissan, S. Suwas, H.C. Verma: MMM, 263, 307(2003)
8. Jun Ni, T. Ashino, S. Iwata : Acta, 48, 3193(2000)
9. M. Palm, J. Lacaze : Intermetallics,14, 1291(2006)
10. F. Stein, M. Plam, G. Sauthoff: Intermetallics, 13,1056(2005)
11. F. Stein, M. Plam, G. Sauthoff: Intermetallics, 12,713(2004)
12. M. Plam, G. Sauthoff: Intermetallics, 12, 1345(2004)
13. L. Falat, A. Schneider, G. Sauthoff, G. Frommeyer: Intermetallics, 13, 1256(2005)
14. F. Stein, A. Schneider, G. Frommeyer: Intermetallics, 11, 71(2003)

15.R. Ducher, B. Viguier, J. Lacaza : Scripta, 47, 307(2002)

16.U. Prakash 1, G. Sautho : Intermetallics, 9, 107(2001)

17.M. Krasnowski*, H. Matyja : J. Mater. and Com., 319, 296(2001)

18.A. Tokar, A.berner, L. Levin : Mater. Sci. & Eng. A308, 13(2001)

19.R.S. Sundar, T.R.G. Kutty, D.H. Sastry : Intermetallics, 8, 427(2000)

20.R. Kainuma, Y. Fujita, H. Mitsui, I. Ohnuma, K. Ishida : Intermetallics, 8, 855(2000)

21.J. Koike, Y. Shimoyama, I. Ohnuma, R. Kainuma, K. Ishida, K. Maruyama : Acta mater, 48, 2059(2000)

22.A.O. Mekhabov, M.V. Akdeniz : Acta, 7, 2067(1999)

23.S.M. Zhu, K. Iwasaki : Mater. Sci. & Eng., A270, 170(1999)

24.I. Ohnuma, C.G. Schon, R. Kainuma, G. Inden, K. Ishida : Acta, 6, 2083(1998)

25.Y. Nishino, C. Kumada, S.Asano : Scripta, 4, 461(1997)

26.R.Kainuma, K. Urushiyama, K. Ishikawa, C.C. Jia, I. Ohnuma, K. Ishida : Mater. Sci. & Eng., A239-240, 235(1997)

27.L. Machon & G. Sauthoff : Intermetallics, 4, 469(1996)

28.M. Palm, G. Inden, N. Thomas : J. Phase Equilibria, 16, No. 3, 209(1995)

29.L. Anthony, B. Fultz : Acta metall. Mater., 43, No. 10, 3885(1995)

30.C.H. Sellers, T.A. Hyde, T.K. O'Brien, R. N. Wright : J. Phys. Chem. Solids, 55, 505(1994)

31.D. Lin, A. Shan, D. Li : Scripta, 11, 1455(1994)

32.G, Inden, W. Pepperhoff : Z. Metallkde, 81, 770(1990)

33.S.M. Zhu, K. Sakamoto, M. Tamura, K. Iwasaki : Mater. trans., 42, 484(2001)

34.A. Gorzel, M. Palm, G. Sauthoff : Z. Metallkd. 90, 64(1999)

35.D.G. Morris, L.M. Requejo and M.A. Muñoz-Morris : Intermetallics, 13, 862(2005)

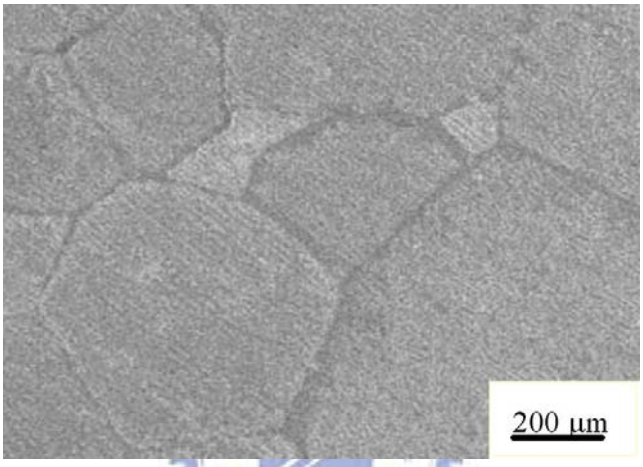

Figure 1

Figure 1. An optical micrograph of the as-quenched alloy

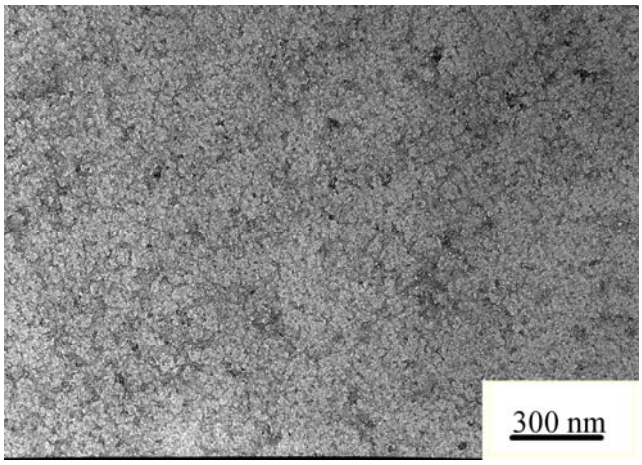

Figure 2(a)

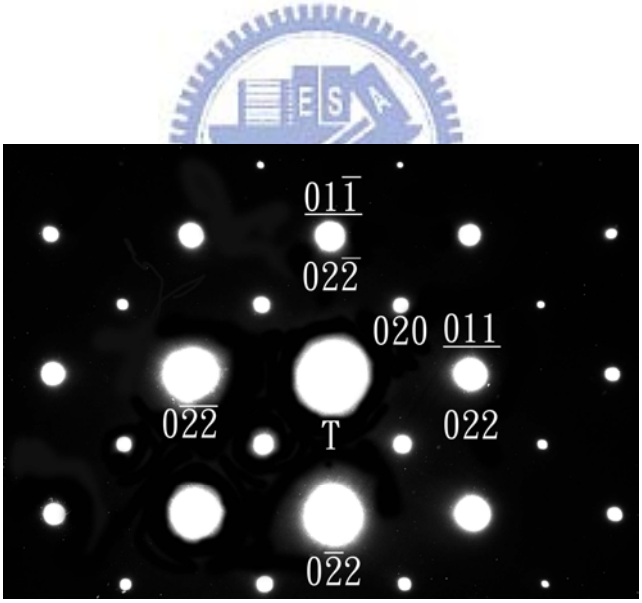

Figure 2(b)

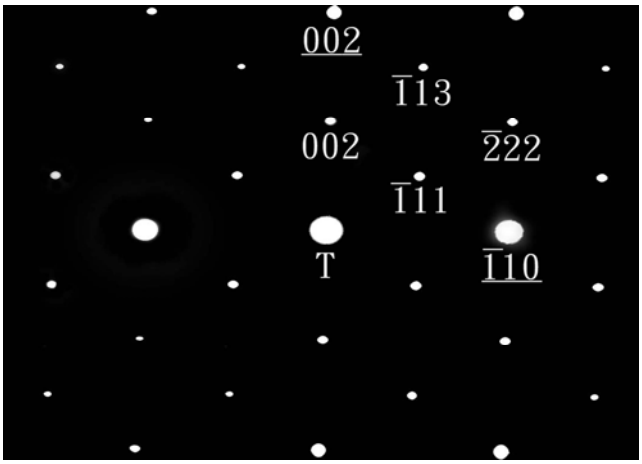

Figure 2(c)

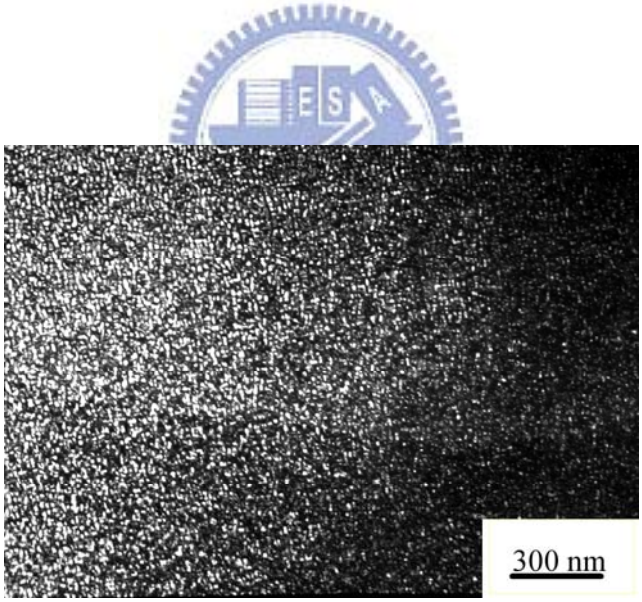

Figure 2(d)

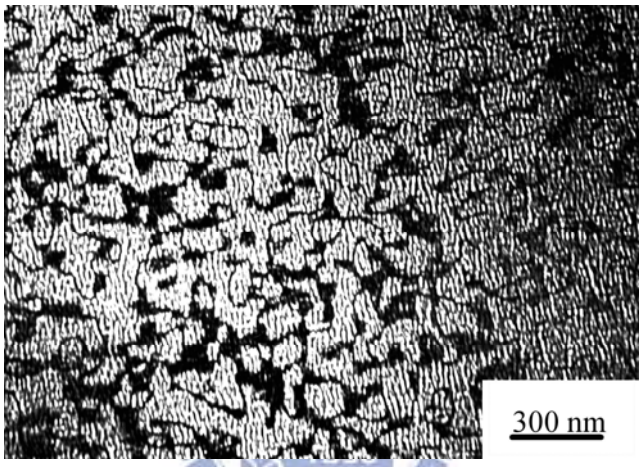

Figure 2(e)

Figure 2. Electron micrographs of the as-quenched alloy, (a) BF, (b) and (c) two selected-area diffraction patterns (SADPs) taken from the matrix. The zone axes are [100] and [110], respectively. (hkl = α phase; $\underline{hkl}$ = $D0_3$ phase) (d) and (e) ($\bar{1}11$) and (002) $D0_3$ DF electron micrographs, respectively.

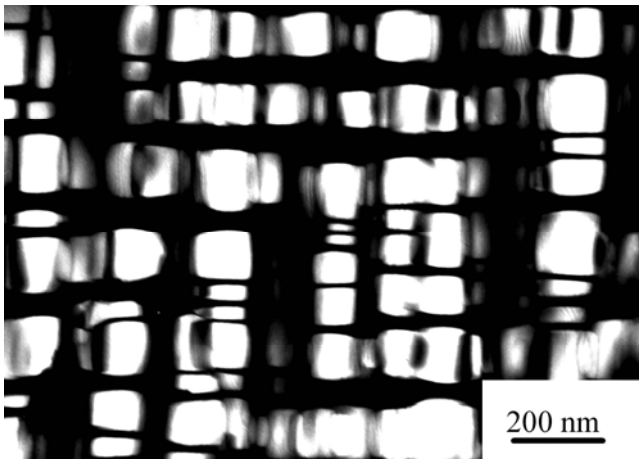

Figure 3(a)

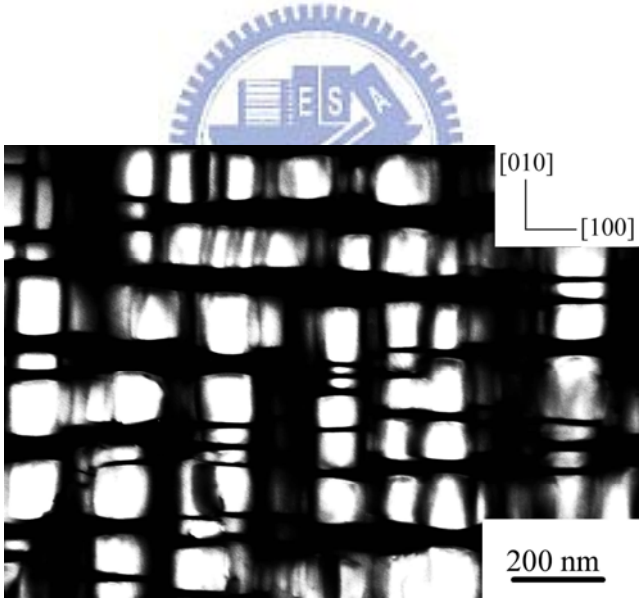

Figure 3(b)

Figure 3. Electron micrographs of the alloy aged at 700℃ for 6 hours, (a) and (b) $(\bar{1}11)$ and (002) $D0_3$ DF electron micrographs, respectively.

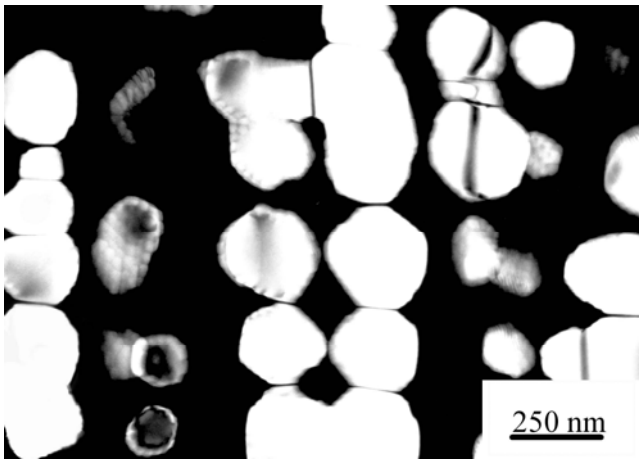

Figure 4(a)

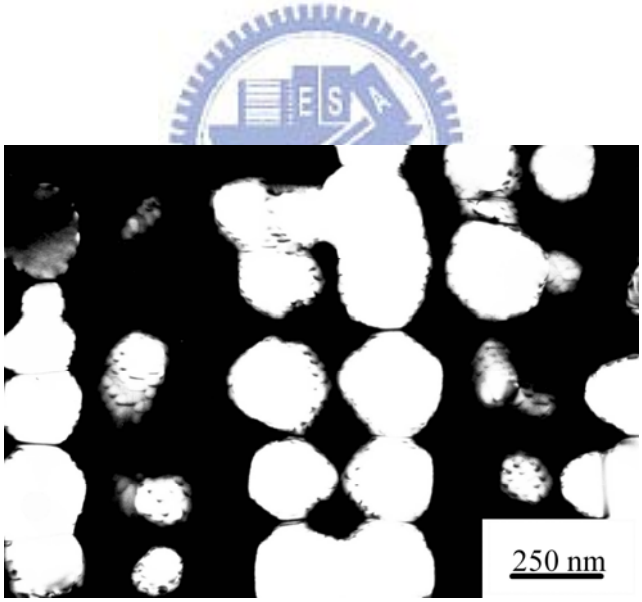

Figure 4(b)

Figure 4. Electron micrographs of the alloy aged at 700℃ for 12 hours, (a) and (b) ($\bar{1}11$) and (002) $D0_3$ DF electron micrographs, respectively.micrographs, respectively.

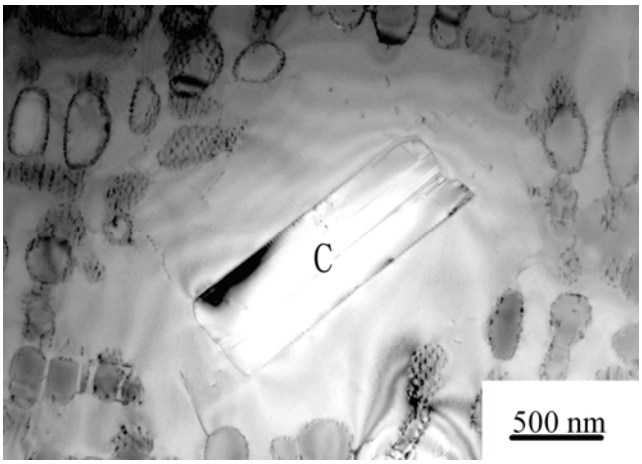

Figure 5(a)

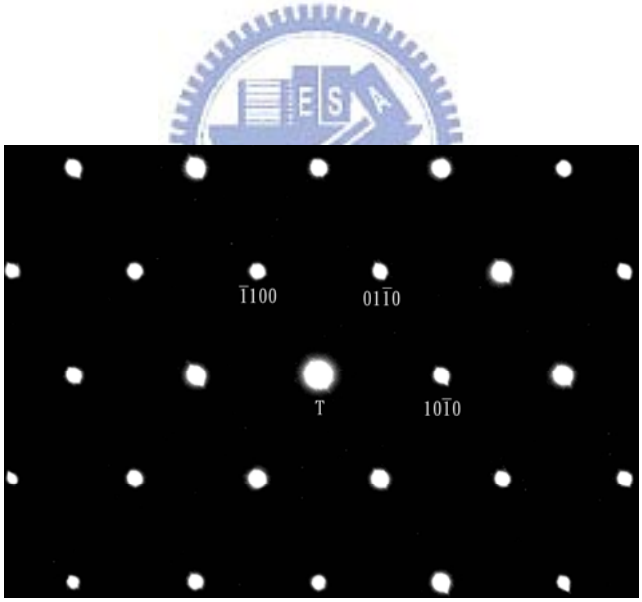

Figure 5(b)

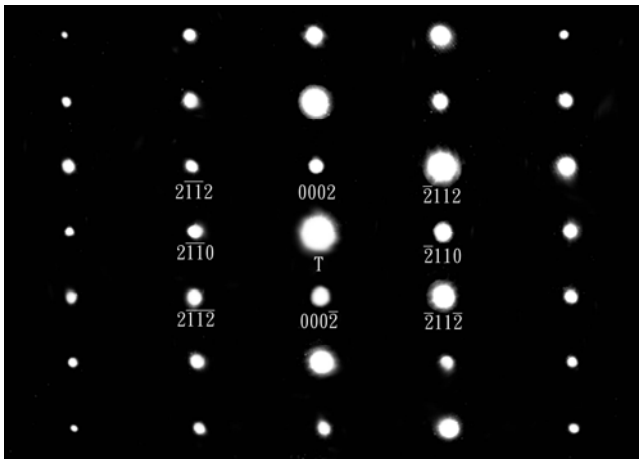

Figure 5(c)

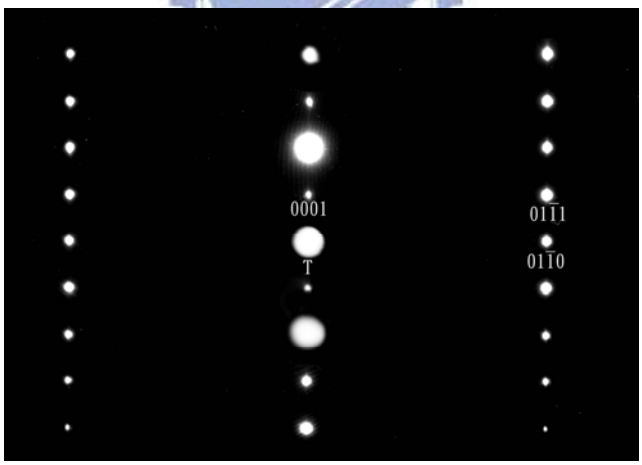

Figure 5(d)

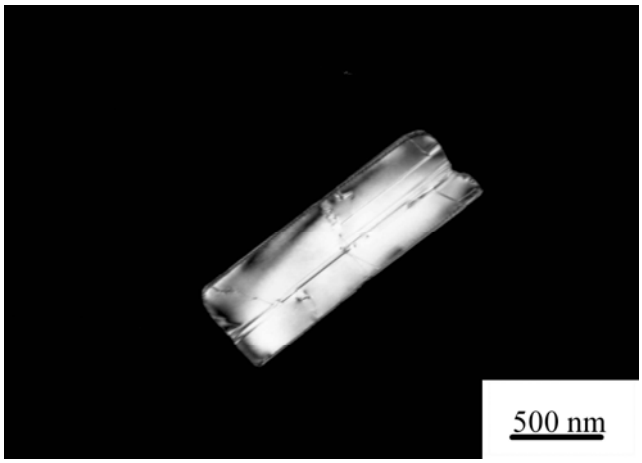

Figure 5(e)

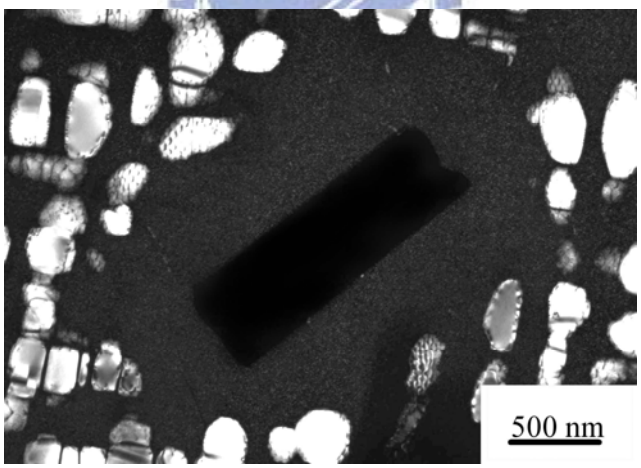

Figure 5(f)

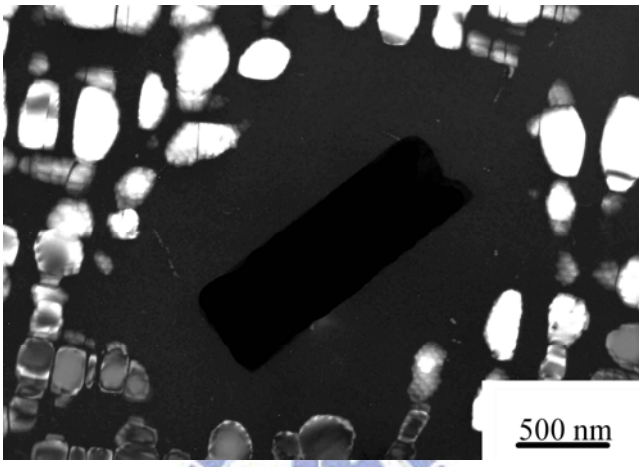

Figure 5(g)

Figure 5. Electron micrographs of the alloy aged at 800℃ for 0.5 hour, (a)BF, (b) through (d) three SADPs taken from the rod-like precipitate marked as C in (a). The foil normals are [0001], $[0\bar{1}\bar{1}0]$ and $[2\bar{1}\bar{1}0]$, respectively. (hkil = C14 precipitate; <u>hkl</u> = $D0_3$ phase) (e)C14 DF, (f) and (g) $(\bar{1}11)$ and (002) $D0_3$ DF electron micrographs, respectively.

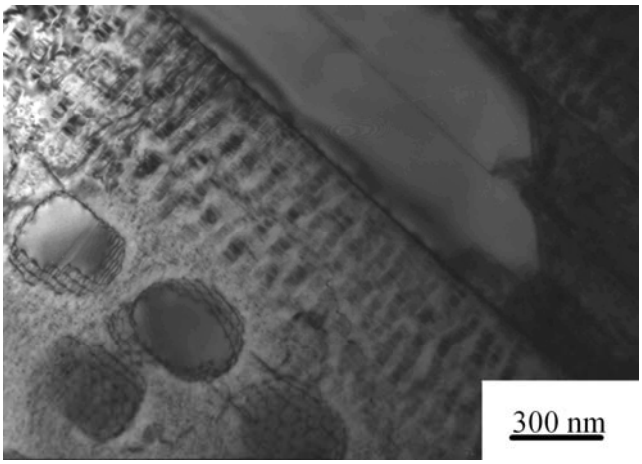

Figure 6(a)

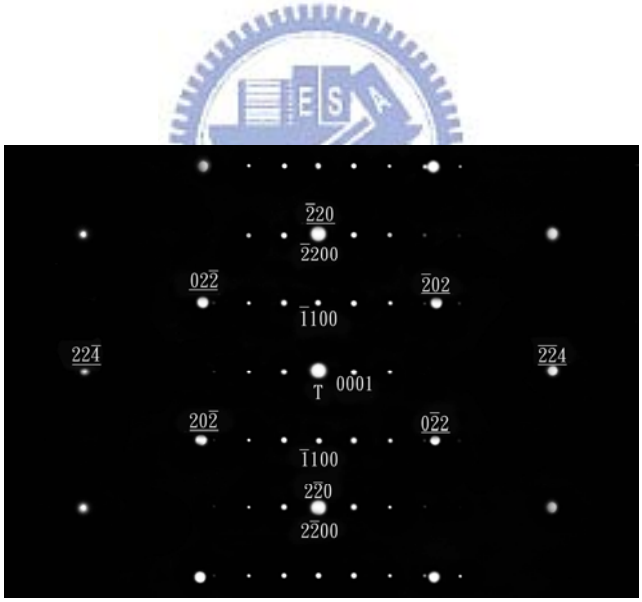

Figure 6(b)

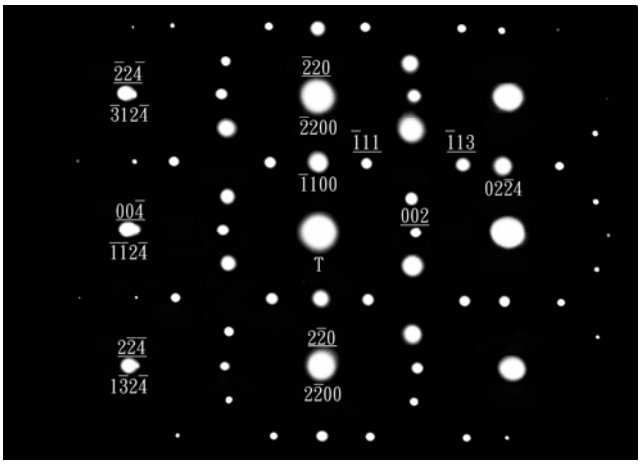

Figure 6(c)

Figure 6(d)

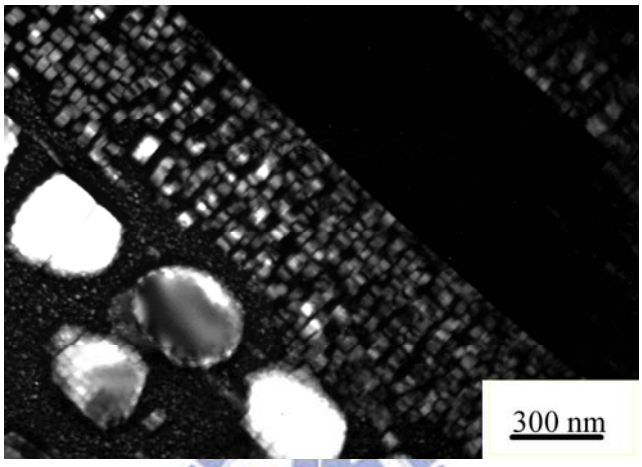

Figure 6(e)

Figure 6. Electron micrographs of the alloy aged at 800℃ for 1 hour, (a)BF, (b) through (d) three SADPs taken from an area including the C14 precipitate and its surrounding matrix. The zone axes of the (A2+$D0_3$) matrix are (b) [1 1 1], (c) [1 1 0], (d) [$\bar{1}$ $\bar{1}$ 2], respectively. (hkil = C14 precipitate; <u>hkl</u> = $D0_3$ phase), (e) ($\bar{1}$11)$D0_3$ DF.

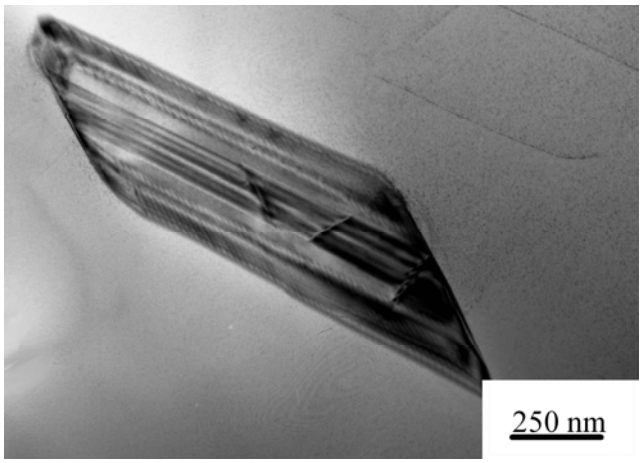

Figure 7(a)

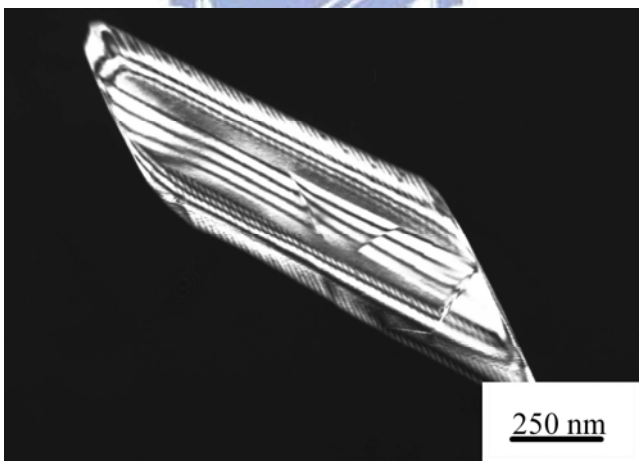

Figure 7(b)

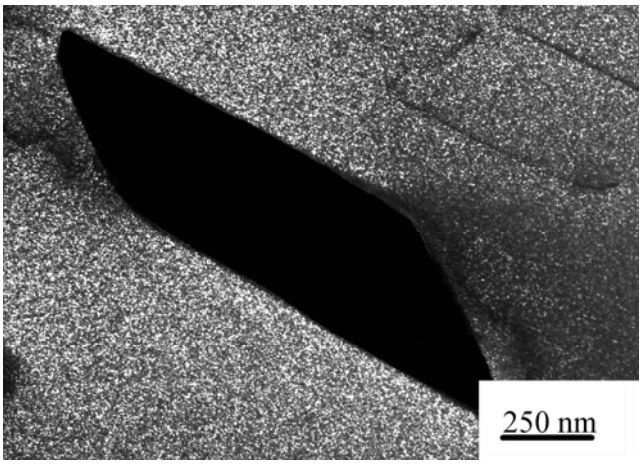

Figure 7(c)

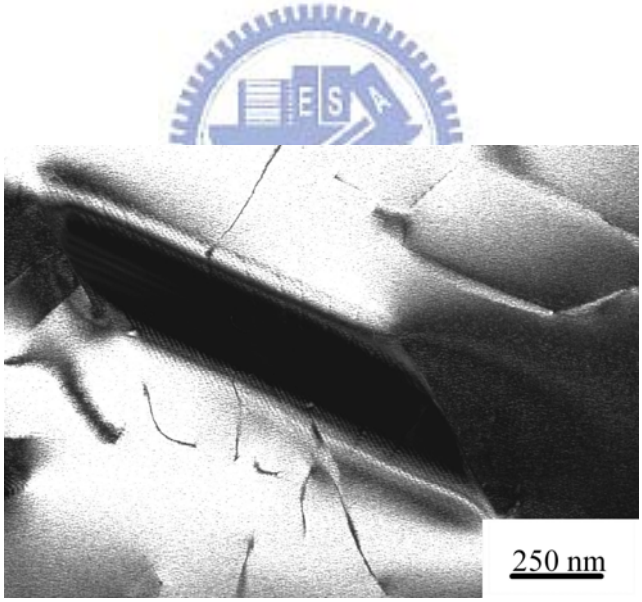

Figure 7(d)

Figure 7. Electron micrographs of the alloy aged at 900℃ for 6 hours, (a) BF, (b) C14 DF, (c) and (d) ($\bar{1}11$) and (002) $D0_3$ DF electron micrographs, respectively.

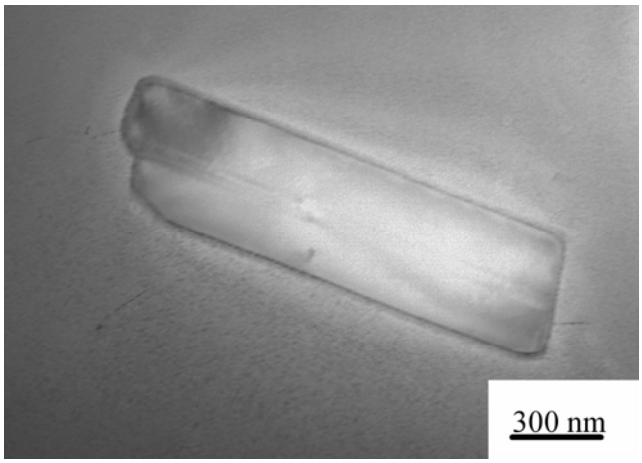

Figure 8(a)

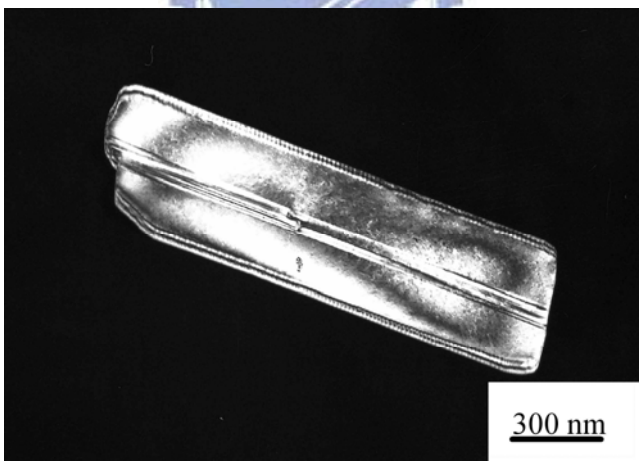

Figure 8(b)

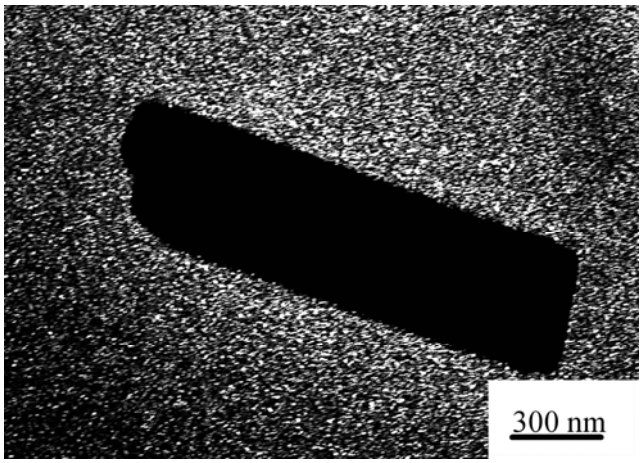

Figure 8(c)

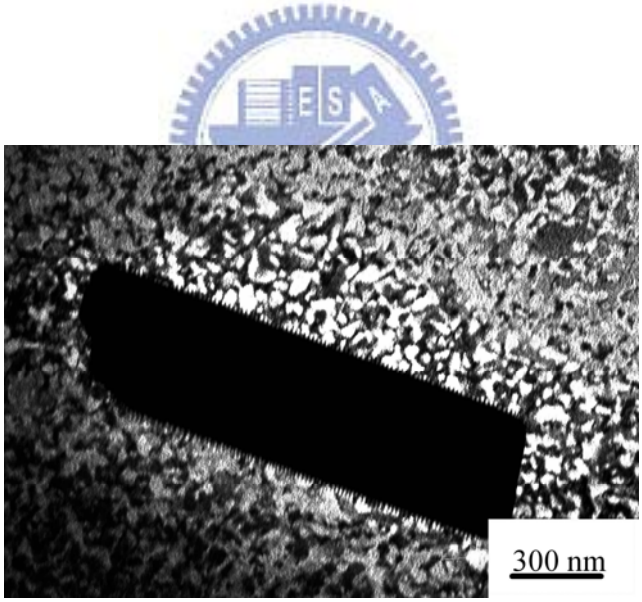

Figure 8(d)

Figure 8. Electron micrographs of the alloy aged at 1000℃ for 1 hour, (a)BF, (b)C14 DF, (c) and (d) ($\bar{1}11$) and (002) $D0_3$ DF electron micrographs, respectively.

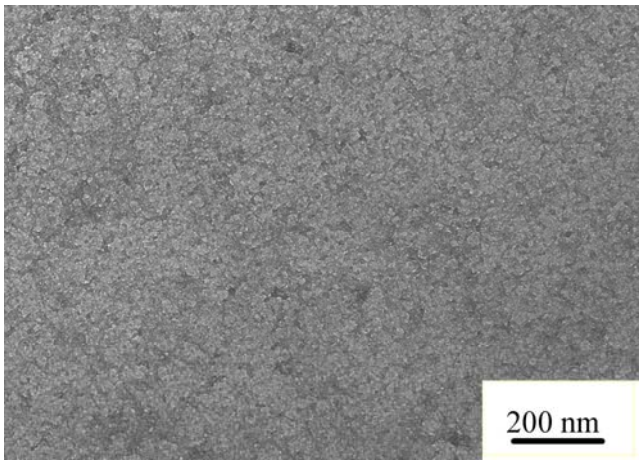

Figure 9(a)

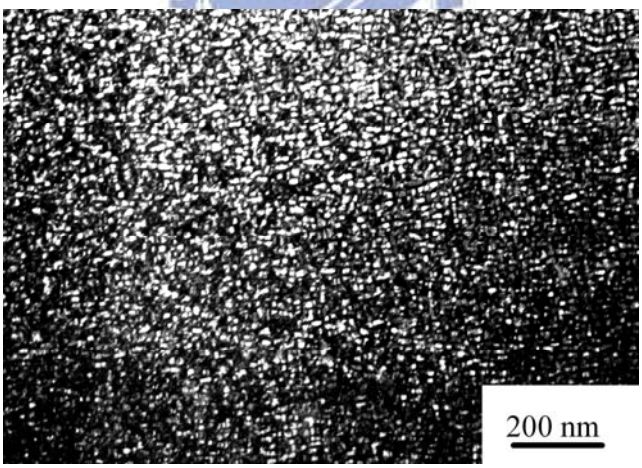

Figure 9(b)

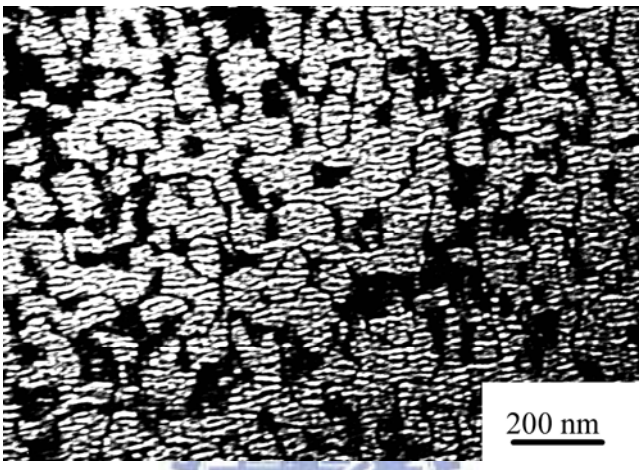

Figure 9(c)

Figure 9. Electron micrographs of the alloy aged at 1100℃ for 1 hour, (a)BF, (b) and (c) ($\bar{1}11$) and (002) $D0_3$ DF electron micrographs, respectively.

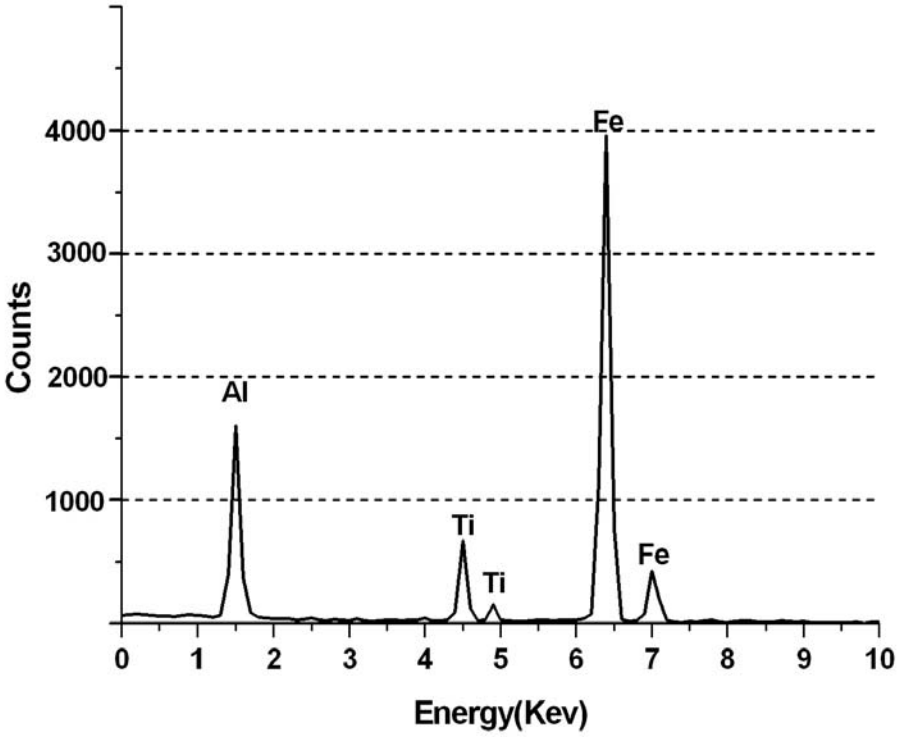
Counts
4000
3000
2000
1000
Al
Ti
Ti
Fe
Fe
0
1
2
3
4
5
6
7
8
9
10
Energy(Kev)

Figure 10(a)

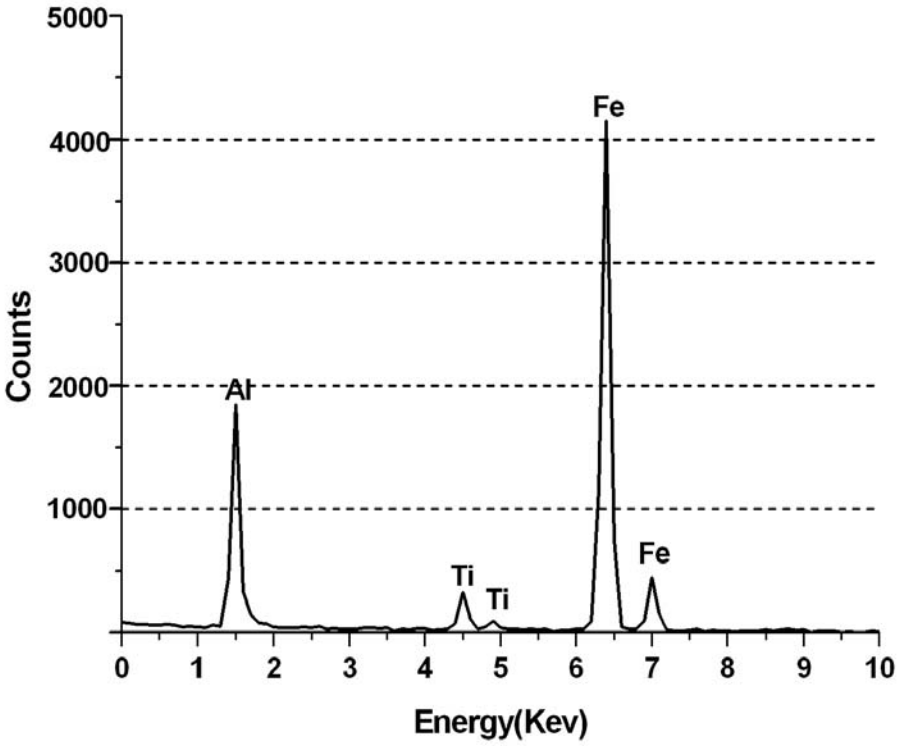
5000
4000
3000
2000
1000
Counts
Al
Ti
Ti
Fe
Fe
0
1
2
3
4
5
6
7
8
9
10
Energy(Kev)

Figure 10(b)

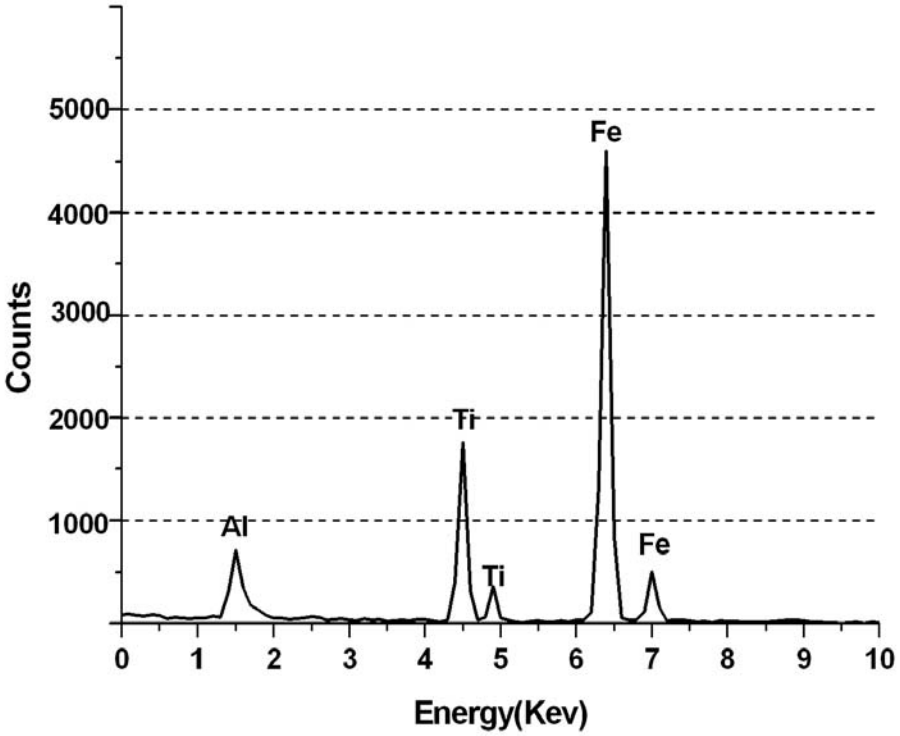
Counts
5000
4000
3000
2000
1000
Fe
Ti
Al
Ti
Fe
0
1
2
3
4
5
6
7
8
9
10
Energy(Kev)

Figure 10(c)

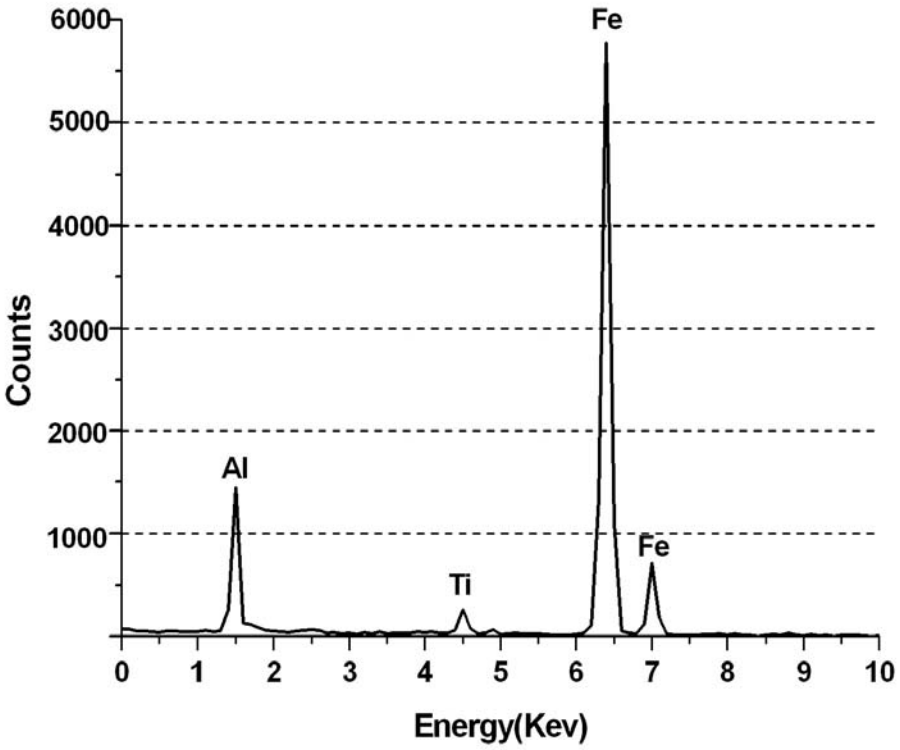

Figure 10(d)

Figure 10.(a) through (d) four typical EDS spectra taken from a granular-like $D0_3$ particle within the matrix, a cuboidal $D0_3$ particle contiguous to the C14 precipitate, C14 precipitate and the (A2+$D0_3$) matrix in the alloy aged at 800˚C for 1 hour, respectively.

Table 1. Chemical compositions of the phases revealed by Energy-Dispersive Spectrometer(EDS)

Heat Treatment	Phase	Fe(at.%)	Al(at.%)	Ti(at.%)
Solution heat-treated (1150℃/1hr.)	A2	71.81	18.09	10.10
800℃/1hr. Aging	granular-like $D0_3$	65.23	23.47	11.30
	cuboidal $D0_3$	67.35	26.11	6.54
	C14	63.98	10.37	25.65
	A2+$D0_3$	78.25	16.99	4.76